MAY 1965

<u>Cooling of Neutron Stars</u>

by

Sachiko Tsuruta

Smithsonian Astrophysical Observatory
Cambridge, Massachusetts

and

A.G.W. Cameron

Institute for Space Studies
Goddard Space Flight Center, NASA
New York, New York

The discovery of discrete sources of x-rays[1] in the sky has led to much speculation as to the mechanisms responsible for the x-ray emission[2-6]. Among these suggestions has been the thermal emission of x-rays from the hot surfaces of neutron star remnants of supernova explosions[2,3]. Calculations of the cooling of such a neutron star following its formation have seemed to indicate that the temperature would still be several million degrees at an age of several thousand years. Such cooling calculations have been based upon estimates of photon emission from the surface and of neutrino-antineutrino pair emission by the plasma process from the interior. There have recently been new suggestions regarding other possible mechanisms of neutrino emission from the interior[7], and this has led to the impression that neutron stars might cool too rapidly to be observable as celestial x-ray objects[5,8]. We believe this view to be overly pessimistic, and we give here a brief summary of some of our cooling calculations for neutron stars.

The neutron star models we have used in our calculations have been based upon composite equations of state with nuclear forces included. The details of the construction of the equations of state have been described in a thesis[3], and will be published in due course. At the lowest densities, but still at substantially high temperatures, the composition was assumed to be iron. As the density increases, the main contribution to the pressure comes from the degenerate electrons, and the mean molecular weight per electron gradually increases as the high Fermi level of the electrons forces the nuclear composition of the material to change toward higher mass number. At densities between 10^{11} and 10^{14} gm/cm^3 the heavy nuclei gradually dissolve into neutrons. The system then consists of degenerate neutrons, protons and electrons. Near and above 10^{15} gm/cm^3, many other particles appear in the mixture, commencing with the μ meson and the Σ^- hyperon. In constructing our equations of state, the degeneracy pressures of all the individual fermions were added, and nuclear force terms were also included.

Nuclear forces are generally attractive at large internucleon distances and repulsive at small internucleon distances. In this work we chose forms of the potential interactions between neutrons suggested by Levinger and

Simmons[9]. Their potentials V_β and V_γ were utilized. Both of these potentials are attractive at low densities, although V_γ is somewhat more attractive than V_β. At high densities V_γ rapidly turns repulsive, while V_β only slowly turns repulsive. For our neutron star equations of state, we have applied these potentials between the baryons without distinction as to the type of baryon. At densities less than or equal to nuclear densities, the character of nuclear forces is reasonably well known and is given to a rough approximation by either of these potentials, and the composition of the matter is mostly neutrons, for which the potentials were originally constructed. At much greater than ordinary nuclear densities many different types of baryon are present, and the rapidity with which nuclear forces turn repulsive is very speculative. Hence the two potentials V_β and V_γ tend to span a range of possible behavior of the nuclear forces at high densities, and the differences in the neutron star models which result from the adoption of one or the other potential will give an indication of the uncertainty due to lack of knowledge in this area of physics.

In the case of a perfect fluid there is a general relativistic limitation on the pressure such that it cannot exceed one-third of the proper energy density[10]. In a fluid with suitable anisotropic properties, this condition may be violated, but the ultimate relativistic condition still remains that the pressure cannot exceed the proper energy density[11]. If this were to be violated the speed of sound would exceed the speed of light in the medium. Accordingly, the composite equation of state constructed as described above was cut off with one of these two pressure saturation conditions.

The general relativistic equations of hydrostatic equilibrium were derived by Oppenheimer and Volkoff[12]. For a given assumption about central density, the numerical integration of the differential equations of hydrostatic equilibrium gives models with uniquely determined masses. The gravitational and proper masses determined in this way as a function of central density for the two composite equations of state are shown in Figure 1. Several interesting comments follow from this figure. It is evident that the details of the structure of the neutron star models are very sensitive to the uncertainties in the rate at which nuclear repulsive forces enter in the baryon mixture at high densities. For each equation of state the mass rises with increasing central density toward a principal peak, beyond which it falls and then oscillates. It is interesting to note that the gravitational mass is less than the proper mass over the entire range of neutron star models, thus showing that such models are gravitationally bound. This is contrary to the behavior of models constructed with non-interacting neutron gases. An expanded discussion of the stability of the models beyond the main peak will be given separately[13,14]. It may also be noted that pressure saturation does not set in until the vicinity of the principal peak has been reached. Hence uncertainties in the pressure saturation effects play no significant role in the discussion which follows.

In order to calculate representative cooling curves for neutron star models, three models were chosen so that one was of low mass at the low density base of the principal peak, one was halfway up the peak, and the other was near the top of the peak. To these models were fitted hot atmospheres corresponding to a series of surface temperatures. These atmospheres were composed of both iron and magnesium; the results were nearly the same and only the neutron stars with iron envelopes are discussed here. It was typically found that the temperature rose by about a factor 50 between the photosphere of the neutron star and the interior where the high thermal conductivity of the electrons assured a flat temperature distribution. The atmospheres were constructed with the help of opacities calculated from the Los Alamos opacity code of A.N. Cox and his collaborators. The atmospheric structure was determined by requiring that the luminosity should not change from one layer to the next.

The heat capacity of the neutron star models is a function of their temperature[15]. The presence of nuclear forces in the equation of state will modify the heat capacity by an amount which typically can be of the order of a factor 2, according to rough estimates which we have made. We did not take such modifications into account in making the actual cooling calculations.

The cooling of the neutron stars is due to the combination of neutrino emission from the interior and photon emission from the surface. The construction of the envelope automatically provided us with the photon cooling rates. Three neutrino cooling rates were taken into account, as follows:

(1) Neutrino pair emission from the plasma process. These neutrinos arise from the decay of plasmons in the degenerate electron gas in the interior of the neutron star. The rates have been given by Adams, Ruderman, and Woo and by Inman and Ruderman[16].

(2) The URCA process. Bahcall and Wolf have recently given an estimate of neutrino emission from this process[8], in which neutrons decay into protons and protons capture electrons. The rate is somewhat greater than that of the plasma process.

(3) The neutrino bremsstrahlung process. The neutrino pairs are emitted when electrons scatter from positive or negative baryons in the interior of the neutron star. Ruderman and Festa have kindly provided us with the following approximate preliminary expression for this process[17]:

$$q\left(\frac{\text{ergs}}{\text{gm-sec}}\right) = 10^6 \; Z^2 \; \frac{n_z}{n} \quad (T_9)^6$$

$$\text{for} \quad E_F >> mc^2$$

where Z is the effective charge of the electron scattering centers, n_z is the number density of such centers, and n we take here to be the baryon number density. Ruderman and Festa have suggested that there may be proton clustering in neutron star interiors in the presence of very large numbers of neutrons, so that the effective charge of scattering center might be 2. However, it may well be that under conditions of interest in the interiors of neutron stars there will also be large number of Σ^- hyperons, which may hinder the clustering process. Consequently, we have chosen to take the effective charge of a scattering center equal to unity and to count as the scattering centers both the protons and the Σ^- hyperons. This process is less important than the URCA process at high temperatures, but it is more important at low temperatures.

The cooling curves for the six chosen neutron star models as a function of age are shown in Figure 2. It may be seen that the rate of cooling has a significant dependence on the mass of the star. The low mass stars cool quite rapidly, but the medium and heavy mass stars still have temperatures exceeding 2×10^6 °K for times of the order of 10^4 or 10^5 years. Hence it is evident that thermal emission of x-rays from neutron star surfaces should continue to be regarded as candidates for identification with some of the x-ray sources which are being found in the sky.

Bahcall and Wolf have raised the question of neutrino cooling from pion decays in neutron star interiors. Such pion decays can occur only if pions should have a small effective mass in the presence of a largely neutron gas. Both Bahcall and Ruderman have indicated to us (private communications) their expectations that, under the conditions in which pions may be present in a neutron star, there will be a predominantly repulsive interaction between the pions and the neutrons. This would raise rather than lower the effective mass of the pions, and make it very unlikely that pions will be present in the interiors of neutron stars on the low density side of the principal peak.

The remarkable NRL rocket experiment carried out during a lunar occultation of the Crab Nebula has shown that the x-ray source associated with the Crab Nebula has dimensions very much larger than those of a neutron star. One of us has suggested that these x-rays may be due to the synchrotron process from high energy electrons accelerated in the magnetosphere of a vibrating neutron star[6]. Similar nonthermal processes may well be associated with other x-ray sources, if they are neutron stars, and hence nonthermal components to x-ray spectra may be common. Hence we believe that many more highly refined experiments will be necessary before the true nature of the celestial x-ray sources will be determined.

We are grateful to Dr. Ruderman and Mr. Festa for communicating to us in advance of publication their preliminary results on neutrino emission by the bremsstrahlung process.

Bibliography

[1] R. Giacconi, H. Gursky, F.R. Paolini, and B.B. Rossi, Phys. Rev. Letters, 9, 439 (1962); Phys. Rev. Letters, 11, 530 (1963); S. Bowyer, E.T. Byram, T.A. Chubb, and H. Friedman, Nature, 201, 1307 (1964); Science, 146, 912 (1964); P.C. Fisher, A.F. Meyerott, Astrophys. J., 139, 123 (1964).

[2] H.Y. Chiu, and E.E. Salpeter, Phys. Rev. Letters, 12, 412 (1964); D.C. Morton, Nature, 201, 1308 (1964); D.C. Morton, Nature, 201, 1308 (1964); C.W. Misner and H.S. Zapolsky, Phys. Rev. Letters, 12, 635 (1964); A. Finzi, Astrophys. J., 139, 1398 (1964).

[3] S. Tsuruta, Thesis, Columbia Univ. (1964).

[4] P. Morrison, Second Sympsoium on Relativistic Astrophysics, Austin, 1964 (to be published).

[5] G.R. Burbidge, R.T. Gould, and W.H. Tucker, Phys. Rev. Letters, 14, 289 (1965).

[6] A.G.W. Cameron, Nature, 205, 878 (1965).

[7] For instance π^- processes as suggested in reference 8, and bremsstrahlung processes as given in reference 17.

[8] J.N. Bahcall and R.A. Wolf, Phys. Rev. Letters, 14, 343, (1965).

[9] J.S. Levinger, and L.M. Simmons, Phys. Rev., 124, 916 (1961).

[10] L. Landau, and E. Lifshitz, The Classical Theory of Fields, Addison-Wesley (1959).

[11] Ya.B. Zel'dovich, JETP, 14, 1143 (1962).

[12] J.R. Oppenheimer, and G.M. Volkoff, Phys. Rev., 55, 374 (1939).

[13] S. Tsuruta, J. Wright, and A.G.W. Cameron, (to be published).

[14] S. Tsuruta, accompanying paper.

[15] S. Chandrasekhar, Introduction to the Study of Stellar Structure, Dover (1957).

[16] J.B. Adams, M.A. Ruderman, and C.H. Woo, Phys. Rev., 129, 1383 (1963); C.L. Inman and M.A. Ruderman, Astrophys. J., 140, 1025 (1964).

[17] M.A. Ruderman and G. Festa, private communication (1965).

FIGURE CAPTIONS

Figure 1: Gravitational and proper masses of the neutron star models constructed with both composite equations of state and plotted as a function of central density. The different models resulting from the two pressure saturation conditions at the highest densities are separately indicated.

Figure 2: The cooling curves for selected neutron star models fitted with atmospheres of iron, with three models for each composite equation of state. In the portions of the curves to the left of the crosses cooling occurs predominantly by neutrino emission from the interior; to the right of the crosses photon cooling from the surface predominates.

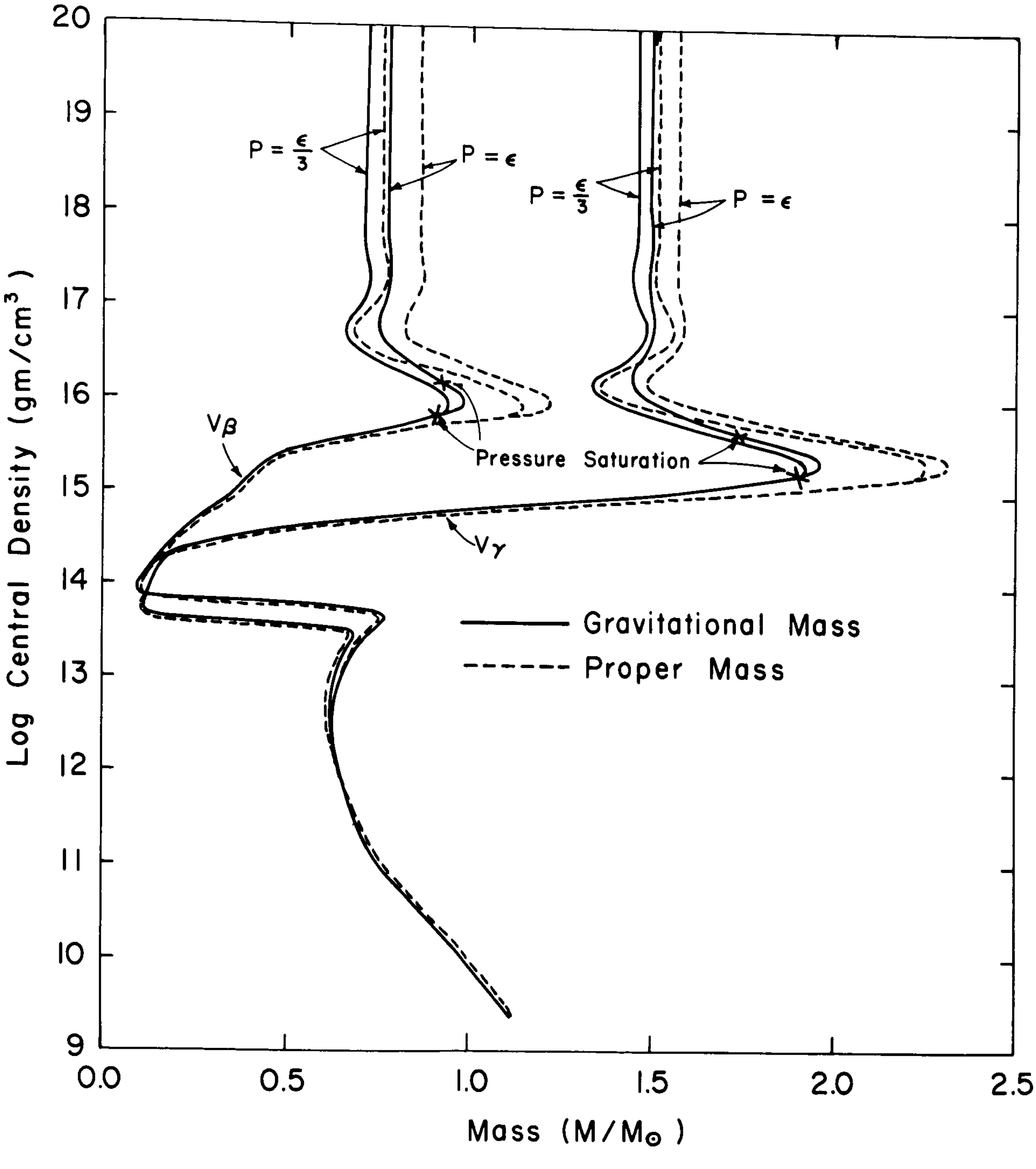

Log Central Density (gm/cm^3)
Mass (M/M$_\odot$)
$P = \frac{\epsilon}{3}$
$P = \epsilon$
$P = \frac{\epsilon}{3}$
$P = \epsilon$
V_β
V_γ
Pressure Saturation
Gravitational Mass
Proper Mass
20
19
18
17
16
15
14
13
12
11
10
9
0.0
0.5
1.0
1.5
2.0
2.5

Fig. 1

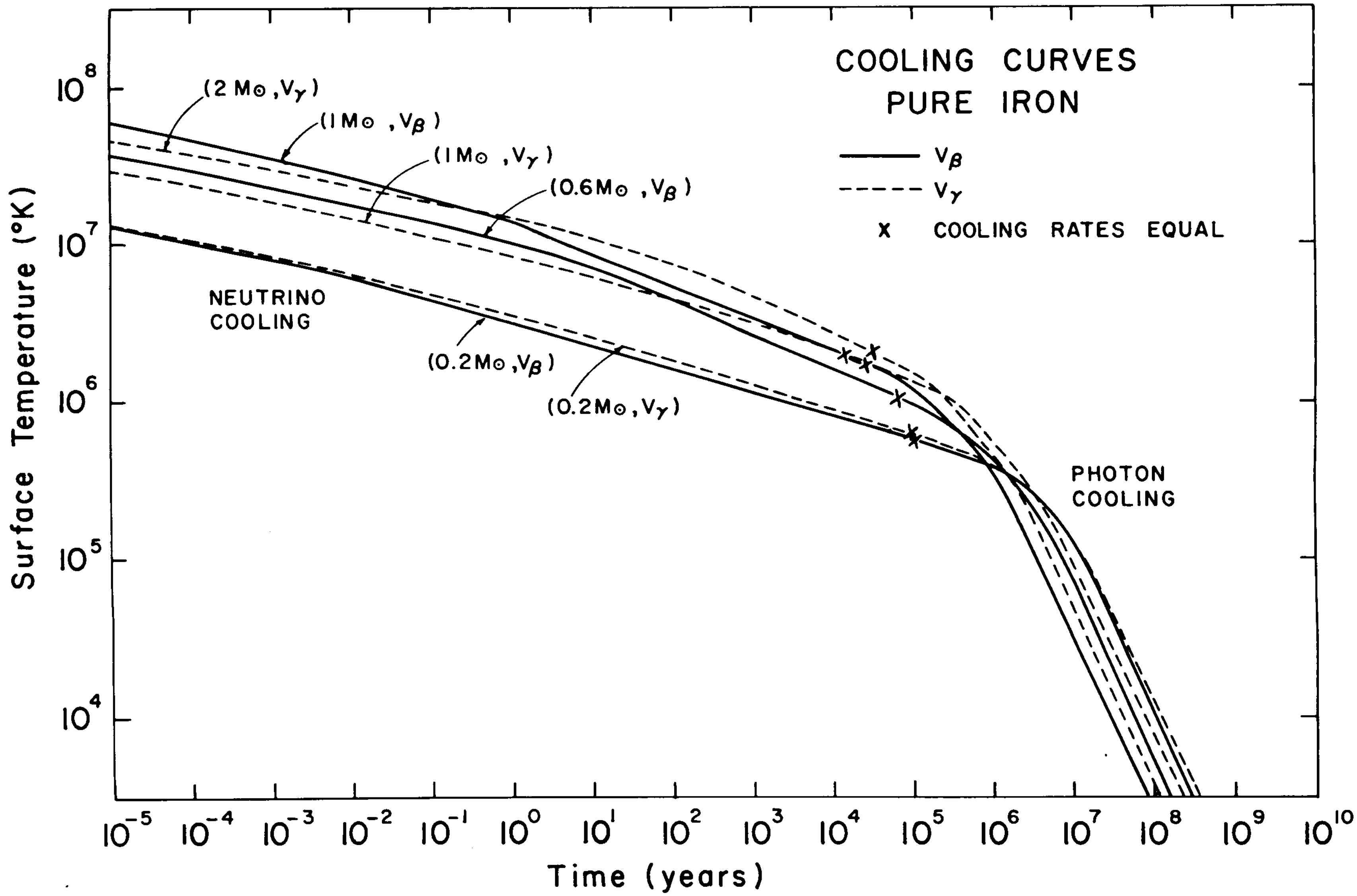
COOLING CURVES
PURE IRON
V_β
V_γ
X COOLING RATES EQUAL
(2 M⊙, V_γ)
(1 M⊙, V_β)
(1 M⊙, V_γ)
(0.6 M⊙, V_β)
(0.2 M⊙, V_β)
(0.2 M⊙, V_γ)
NEUTRINO COOLING
PHOTON COOLING
Surface Temperature (°K)
10^8 10^7 10^6 10^5 10^4
Time (years)
10^{-5} 10^{-4} 10^{-3} 10^{-2} 10^{-1} 10^0 10^1 10^2 10^3 10^4 10^5 10^6 10^7 10^8 10^9 10^{10}

Fig. 2